Arabian Journal of Chemistry (2023) **16**, 104989

King Saud University

Arabian Journal of Chemistry

www.ksu.edu.sa
www.sciencedirect.com

ORIGINAL ARTICLE

Plasma-modified Ni foam-supported $CuCo_2S_4$ nanowires as bifunctional electrocatalysts for high-performance overall water splitting

Yongjun Shen [a,b,*,1], **Yin Chen** [b,1], **Shuaikang Fang** [b], **Jae Kwang Park** [c], **Kun Feng** [a]

[a] *Research Center of Secondary Resources and Environment, School of Chemical Engineering and Materials, Changzhou Institute of Technology, Changzhou 213022, China*
[b] *School of Chemistry and Chemical Engineering, Nantong University, Nantong 226019, China*
[c] *Department of Civil and Environmental Engineering, University of Wisconsin–Madison, 1415 Engineering Drive, Madison, WI 53706, USA*

Received 2 April 2023; accepted 8 May 2023
Available online 12 May 2023

KEYWORDS

Plasma-modified;
Copper cobalt sulfide;
Ni foam;
Water splitting;
Electrocatalyst

Abstract To solve the current energy and environmental dilemma, hydrogen energy is considered to be the best clean energy source to replace traditional fossil fuels. Water electrolysis as the main technology for hydrogen production has been affected by two half-reactions, making it difficult to improve the yield. To solve this problem, the development of inexpensive and efficient bifunctional electrocatalysts is the focus of current research. $CuCo_2S_4$/NF(Ni foam) nanowires are synthesized using a mild hydrothermal process and were later placed in a plasma reactor. Application of the voltage triggers a chemical reaction between the microdischarge wires and the sample. This leads to a change in the physical morphology of the catalyst and an improvement in its catalytic performance. The morphological characterization results show that the catalyst modification generates a distinct flower-like nanowire structure, which helps in the solid attachment of the catalyst to the nickel foam surface. The plasma-modified $CuCo_2S_4$/Ni foam (PA@$CuCo_2S_4$/NF) exhibits low overpotentials of hydrogen evolution reaction (HER) and oxygen evolution reaction (OER) in alkaline solutions. Additionally, the Tafel slopes of the HER and OER are 85.9 $mVdec^{-1}$ and 142.7 $mVdec^{-1}$, respectively, indicating optimal reaction kinetics. A cell voltage of only 1.55 V is required to provide a 10 mA cm^{-2} current during water splitting. This study validates the feasibility of using plasma technology to create high-performance electrocatalysts.

* Corresponding author at: Research Center of Secondary Resources and Environment, School of Chemical Engineering and Materials, Changzhou Institute of Technology, Changzhou 213022, China.
E-mail address: shenyj@czust.edu.cn (Y. Shen).
[1] These authors have contributed equally to this work and considered as co-first authors.

https://doi.org/10.1016/j.arabjc.2023.104989
1878-5352

1. Introduction

Traditional fossil fuels continue to support industrial mass production and basic human energy needs, but they are non-renewable and cause a range of environmental pollution. To address the challenges of energy shortage and environmental pollution, researchers have identified a variety of new energy sources to replace traditional energy sources. In particular, hydrogen energy, with its advantages of being clean, non-polluting and renewable, is receiving increasing attention. Currently, hydrogen production using water electrolysis is the most recognized hydrogen energy production technology (Shang et al., 2020; Wang et al., 2022a,b; Zhu et al., 2020a,b). However, the two half-reactions involved in this process of multiple electron transfer have high activation energies and reaction energy barriers (Liu et al., 2019; Li et al., 2021a,b; Zhang et al., 2021a,b). In order to improve the efficiency of water electrolysis, it is necessary to develop highly reactive, earth-storage rich catalysts favorable to reduce the overpotential (Xiao et al., 2022; Zhu et al., 2022a,b). Presently, the precious metal Pt is the most efficient catalyst for the hydrogen evolution reaction (HER), whereas IrO_2 and RuO_2 are the most efficient catalysts for the oxygen evolution reaction (OER) (Duan et al., 2022; Yang et al., 2020a,b; Zhang et al., 2017). However, their application on an industrial scale is challenging due to high price, poor stability, and low reserves (Chen et al., 2020; Yang et al., 2020a,b). Consequently, the exploration of cheap, highly active and stable bifunctional transition metal electrocatalysts for application in electrolytic water is the most important task at present.

Recently, transition metal sulfides, phosphides, selenides, and nitrides have shown satisfactory electrocatalytic properties for water splitting (Zhang et al., 2020; Yi et al., 2020; Li et al., 2021a,b; Wang et al., 2023a,b; Han et al., 2018) and have emerged as possible contenders for precious metal materials. Among them, most transition metal sulfides have the advantages, such as cost effective, high electrical conductivity, diverse structures, and mild preparation conditions; moreover, the catalytic activity of some transition metal sulfides is comparable to that of the precious metals (Zhang et al., 2023; Guo et al., 2019; Zhang et al., 2021a,b). Zhang et al. reported a layered nanostructure (Ni_3S_2–MoSx/NF) grown directly on nickel foam (Zhang et al., 2019). Ni_3S_2–MoSx/NF exhibited ultralow overpotential and Tafel slope in hydrogen and oxygen evolution reactions and required only 1.54 V to reach 10 mA cm^{-2} in total solution water. Yan et al. synthesized NiCoS nanorods comprising vertical nanosheets by hydrothermal sulfidation; furthermore, its unique structure offered an increased specific surface area and accelerated the charge-transfer rate (Yan et al., 2017). OER tests revealed that NiCoS/NF has an ultralow overpotential of 370 mV at 100 mA cm^{-2}, which indicates the remarkable electrochemical activity of the binary metal sulfide. Yao et al. designed CuS/CF micro nanostructures with superhydrophilic properties. CuS/CF is a bifunctional electrocatalyst with long-lasting stability of 10 h and high catalytic activity (Yao et al., 2022). The selection of suitable substrates is crucial for the stability and catalytic activity of the sample. Currently, three dimensional (3D)-structure of the nickel foam is widely used as a substrate for the in situ preparation of electrocatalytic materials for water splitting. This substrate allows the material to have sufficient active sites, large specific surface area, and high electrical conductivity (Song et al., 2019; Wu et al., 2019; Cen et al., 2021).

Researchers have used various strategies to improve catalyst performance, such as morphology and size modulation, heteroatom doping, and heterostructure engineering (Zhang et al., 2018; Yan et al., 2018; Ma et al., 2022). Compared with these methods, plasma modification is faster and more pollution free. However, few studies have designed bifunctional catalysts using plasma technology. Furthermore, no reports of $CuCo_2S_4$/NF nanowire catalysts modified using plasma have been reported. This chapter describes how we prepared $CuCo_2S_4$/NF nanowire arrays by applying the hydrothermal sulfidation method using nickel foam as the substrate. Subsequently, $CuCo_2S_4$/NF was modified using DBD plasma under atmospheric conditions, and bifunctional catalysts with flower-like nanowires (PA@$CuCo_2S_4$/NF) were obtained. PA@$CuCo_2S_4$/NF exhibited superior electrocatalytic activity for HER and OER, requiring only 107 mV and 110 mV, respectively, as overpotential to drive a current density of 10 mA cm^{-2}. Therefore, we confirmed the feasibility of using DBD plasma technology to design high-performance bifunctional electrocatalysts.

2. Experimental section

2.1. Sample preparation

Copper (II) chloride dihydrate ($CuCl_2{\cdot}2H_2O$, 99%) was provided by Shanghai Maclin Technology Ltd., Co. Cobalt chloride ($CoCl_2{\cdot}6H_2O$, 98%) was supplied by Shanghai Rhawn Chemical Technology Ltd., Co. Urea (CH_4N_2O, 99%), nickel foam (NF, 99%), and sodium sulfide nonahydrate ($Na_2S{\cdot}9H_2O$, 99%) were obtained from Shanghai Aladdin Chemical Technology Ltd., Co. Deionized water was used for the preparation of the materials.

To eliminate any surface impurities, NF with a size of 2 cm × 3 cm was removed and sonicated sequentially in water containing 3 M hydrochloric acid, anhydrous ethanol, and water.

The following steps were taken to produce PA@$CuCo_2S_4$/NF flower-like nanowires. First, the precursors were prepared using the hydrothermal method. A mixture of 0.102 g of $CuCl_2{\cdot}2H_2O$, 0.285 g of $CoCl_2{\cdot}6H_2O$, and 0.36 g of urea was dissolved in a 30 mL of deionized water under magnetic stirring until a homogeneous solution was obtained. Then, a piece of dried NF was placed vertically in a 50 mL reaction kettle and immersed in the mixed solution, ensuring a full contact between the NF and the solution. The reaction kettle was heated at 120 °C for 6 h in an oven. After cooling to room temperature, the CuCo precursor/NF composite was carefully washed, and the nickel foam appeared grayish purple after drying. Then, the precursors were vulcanized. The CuCo precursor/NF composite was placed in a reaction kettle and immersed in a freshly prepared solution of 0.1 mol/L $Na_2S{\cdot}9H_2O$. Furthermore, it was heated to 160 °C and stored in an oven for 8 h. The reaction kettle was opened after complete cooling, and $CuCo_2S_4$/NF composite was obtained by washing it several times and dried overnight. Then, the NF was black.

The plasma modification of $CuCo_2S_4$/NF was performed as follows. A piece of $CuCo_2S_4$/NF material with a size of 1 cm × 1 cm was cut out and placed in the middle of a quartz reactor. The material was fixed between the two electrode plates that were connected to a power supply. The power supply was switched on and adjusted to a certain voltage and current. The air in the reactor was bombarded with plasma to form many active particles that reacted with the catalyst. The samples were plasma bombarded for 60 s to obtain plasma-modified $CuCo_2S_4$/NF, labeled as PA@$CuCo_2S_4$/NF. Where PA stands for Plasma and NF stands for Ni foam.

2.2. Material characterization

The phase composition of the materials synthesized in this thesis was determined using a D8 Advanced X-ray diffractometer manufactured. The X-ray diffractometer uses a Cu-Kα radiation source with a scanning speed of 5° min^{-1}. The morphol-

ogy and composition of the synthesized materials were determined using a Zeiss Gemini 300 scanning electron microscope from Carl Zeiss, Germany, and the elements presented in the samples were analyzed using a scanning electron microscopy (SEM) with an energy dispersive X-ray spectroscopy (EDS). The microscopic morphology of the material was tested by a Philips Tecnai G2 F20 model transmission electron microscope (TEM), and the lattice spacing of the material was obtained from these high-resolution TEM images. To study the surface elements and the valence states of the samples, we utilized a Thermo Kalpha model X-ray photoelectron spectroscopy energy spectrometer from Thermo Fisher for characterization using a monochromated Al Ka source with energy of 1486.6 eV for the tests.

2.3. Electrochemical measurements

Electrochemical tests were conducted using a CHI 660e electrochemical workstation manufactured by Shanghai Chenhua Instrument LTD., Co. The electrochemical workstation was equipped with a three-electrode system. It also had graphite rods as the counter electrode, Ag/AgCl as the reference electrode, and the prepared catalyst (1 cm^2) as the working electrode. Before testing, a 30 mL of the prepared 1 M KOH electrolyte was poured into the electrolytic cell and the electrode clamps were connected. iR compensation of 85% was performed manually, and the linear sweep voltammetry of HER and OER were analyzed at a rate of 0.005 V s^{-1} in the voltage ranges of $-0.9 \sim 0$ V and $1.2 \sim 1.8$ V, respectively; the corresponding Tafel slope was obtained by fitting. The charge-transfer resistance (R_{ct}) of the material was investigated using electrochemical impedance spectroscopy (EIS). HER and OER were measured at voltages of -0.15 V and 1.51 V, respectively, and the frequencies were set from 0.01 to 10^5 Hz. The electrochemical capacitance (C_{dl}) was evaluated using linear cyclic voltammograms (CV) at different sweep rates. Finally, the stability was tested utilizing the chronoamperometry and continuous cyclic voltammetry.

The overall water splitting was mainly tested using the same catalyst for the anode and cathode electrodes in an electrolytic cell with 1 M KOH solution. The polarization curves were tested in the voltage range of 1.1–2.4 V (vs. RHE) to obtain the potential.

3. Results and discussion

3.1. Morphological and structural characterization of $PA@CuCo_2S_4/NF$

CuCo precursors grown directly on 3D NF were synthesized using a hydrothermal method with mild conditions and simple operations, followed by sulfidation via the S^{2-} anions that were released from sodium sulfide (Fig. 1). The resulting $CuCo_2S_4$/NF samples were modified using DBD plasma bombardment on the air in the reactor to produce unique three-dimensional catalysts with flower-like nanowire structures. The color change of the material could be observed throughout this experiment. As shown in Fig. 2, we tested and analyzed the crystal structure information of all samples using an X-ray diffractometer in the range of 20° to 80°. The black curve in the figure illustrates the pure NF, with three distinct

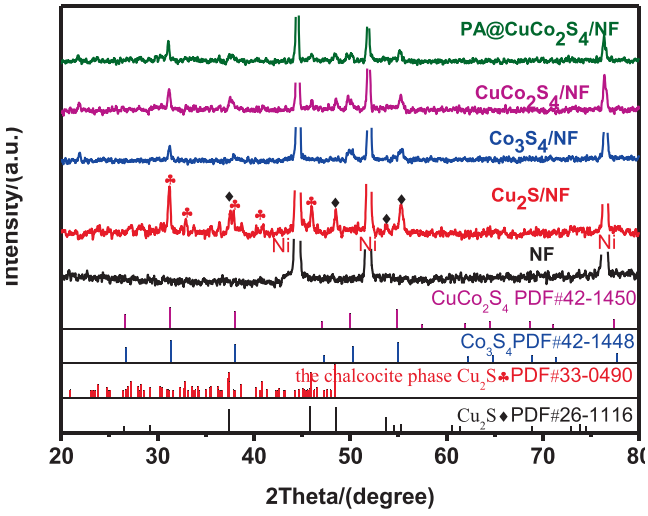

Fig. 2 XRD patterns of NF, Cu_2S/NF, Co_3S_4/NF, $CuCo_2S_4$/NF and $PA@CuCo_2S_4$/NF.

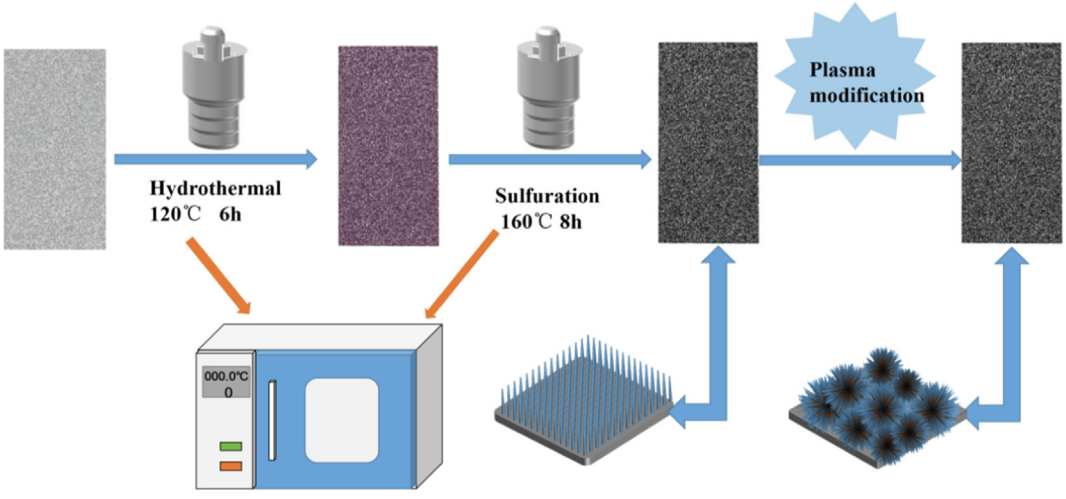

Fig. 1 Schematic illustration of the preparation of the plasma-modified $CuCo_2S_4$/NF nanowire arrays.

diffraction peaks observed at 2θ = 44.6°, 51.7°, and 76.4° corresponding to the (110), (200), and (220) planes of the nickel foam surface, respectively. These three peaks were observed in other samples because the NF was used as the base, and we cropped them to make other peaks more obvious when drawing. More diffraction peaks of Cu_2S/NF corresponding to two PDF cards were present. The diffraction peaks observed at 37.5°, 48.5°, 53.7°, and 55.2° correspond to (102), (103), (112), and (201) planes, which are consistent with the PDF (JCPDS 26-1116) card of Cu_2S. Conversely, the remaining peaks correspond to crystal faces of the chalcocite phase Cu_2S (JCPDS 33-0490), which are (213), (240), (431), (−316), and (630). To differentiate between them, we used black squares and red clubs to mark them on the graph. The blue curve corresponds to the Co_3S_4/NF material. The visible diffraction peaks at 31.3°, 37.9°, 47.3°, 50.1°, and 55.0° in the figure correspond to the (311), (400), (422), (511), and (440) crystal planes of Co_3S_4 (JCPDS 42-1448). The diffraction peaks of $CuCo_2S_4$/NF were very similar to that of Co_3S_4/NF with the peaks at 31.2°, 37.9°, 47.0°, 49.9°, and 54.8° matching with the (113), (004), (224), (115), and (044) planes of $CuCo_2S_4$ (JCPDS 42-1450), indicating that the $CuCo_2S_4$/NF nanowires were successfully prepared. Moreover, the similar diffraction peaks may be due to the identical atomic radii of Cu^{2+} and Co^{2+}, leaving the crystal structure unaltered (Czioska et al., 2018). Meanwhile, we performed XRD tests on the plasma-modified $CuCo_2S_4$/NF. The green curve after the modification showed the same peak as before the treatment, suggesting that the plasma modification did not destroy the crystalline surface of the material.

To understand the mechanisms behind the growth of material on NF and the effect of plasma bombardment on its morphology, we characterized all samples using SEM. As shown in Fig. 3(a–b), we observed the morphology of Cu_2S/NF at 100

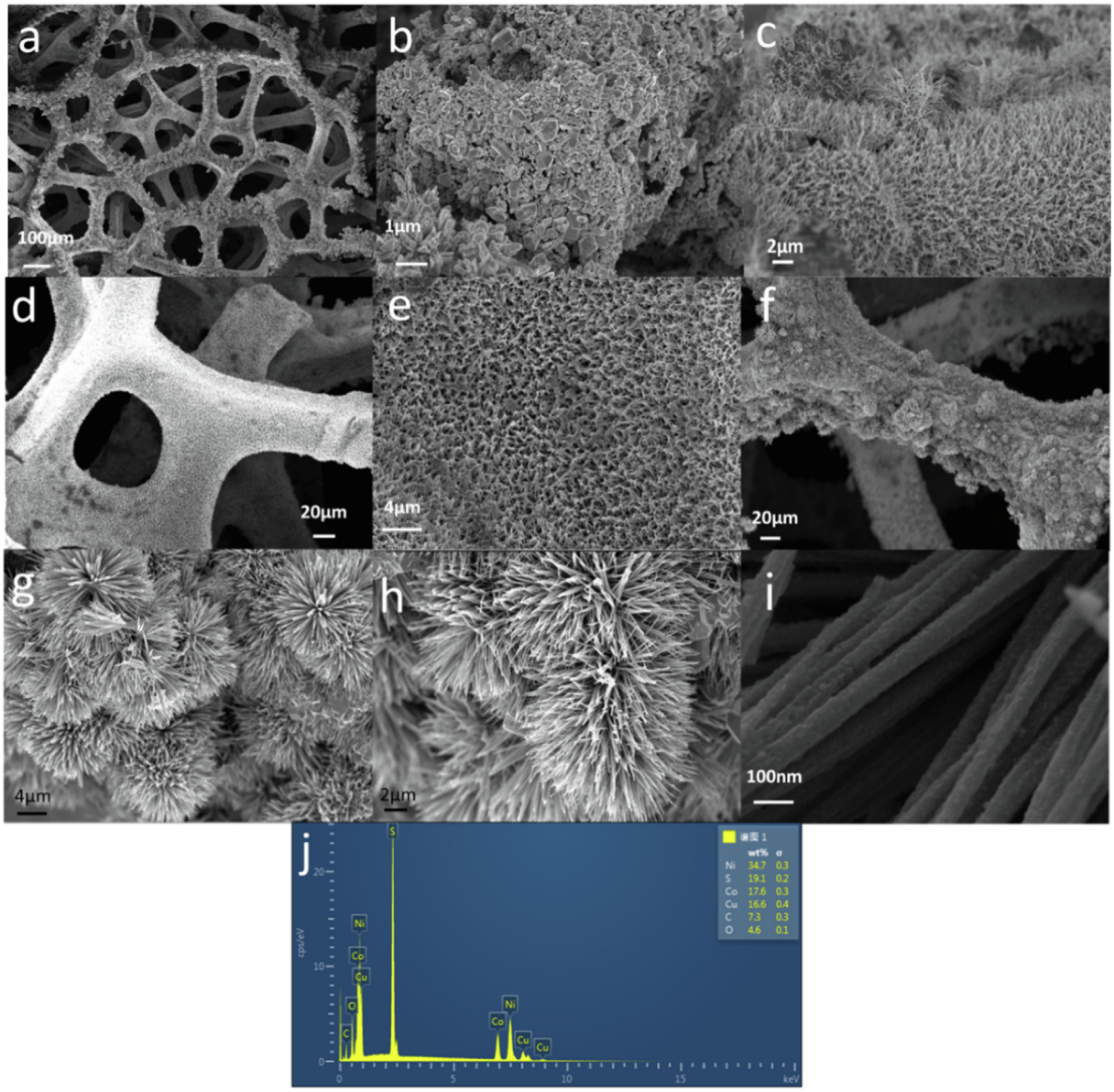

Fig. 3 SEM images of (a–b) Cu_2S/NF, (c) Co_3S_4/NF, (d–e) $CuCo_2S_4$/NF and (f–i) PA@$CuCo_2S_4$/NF. (j) SEM-EDX spectrum of PA@$CuCo_2S_4$/NF nanowire arrays.

and 1 μm. Cu_2S/NF was comprised of irregularly stacked block structures, and it was tightly grown on the 3D network of nickel foam. Fig. 3c shows that the Co_3S_4/NF synthesized without the addition of Cu source formed a regular nanowire structure. Additionally, we found that the $CuCo_2S_4$/NF obtained by adding a Cu source (Fig. 3d–e) exhibited similar nanowire morphology with vertical growth; moreover, fuzziness was observed at 20 μm on the surface of the NF. Fig. 3 (f–i) shows the low- and high-magnification images of the catalyst after plasma modification. From the figure, we observed that the nanowires aggregated to form a flower-like nanowire structure after the plasma bombardment, and a nanoflower grew firmly on the NF in all directions. At higher magnification, pits in the PA@$CuCo_2S_4$/NF nanowires, which were mainly due to plasma bombardments, were observed. This exposed more active sites and facilitated the rapid product transport. The unique flower-like nanowire structure formed by the plasma modification enhances the stability and accelerates the reaction rate. Furthermore, the elemental compositions of PA@$CuCo_2S_4$/NF from the EDX spectra in Fig. 3j showed the presence of Ni, Cu, S, and Co, which again indicates the successful growth of plasma-modified $CuCo_2S_4$ flower-like nanowires on nickel foam.

We further analyzed the microscopic morphology of the plasma-modified $CuCo_2S_4$/NF using TEM. Fig. 4(a–b) show the low-resolution transmission electron micrographs of PA@$CuCo_2S_4$/NF, and we observed that the flower-like structure comprised of nanowires with a diameter of approximately 150 nm, which is consistent with the SEM observation. To further understand the lattice size of the material, we analyzed it using high-resolution transmission electron microscopy imaging (Fig. 4c). After the Fourier calculation, a lattice spacing of 0.28 nm was obtained, which belongs to the (1 1 3) crystal plane of $CuCo_2S_4$ (JCPDS 42-1450). The TEM–EDX spectrogram (Fig. 4d) of PA@$CuCo_2S_4$/NF revealed the presence of Cu, Co, Ni, and S elements, which is in agreement with the results of SEM–EDX. Additionally, we selected a flower-like nanowire area for the high-angle annular dark field and elemental mapping tests. As shown in Fig. 4(e–i), the studies revealed that S, Cu, Ni, and Co were uniformly distributed on the flower-like nanowire structure. The above discussion

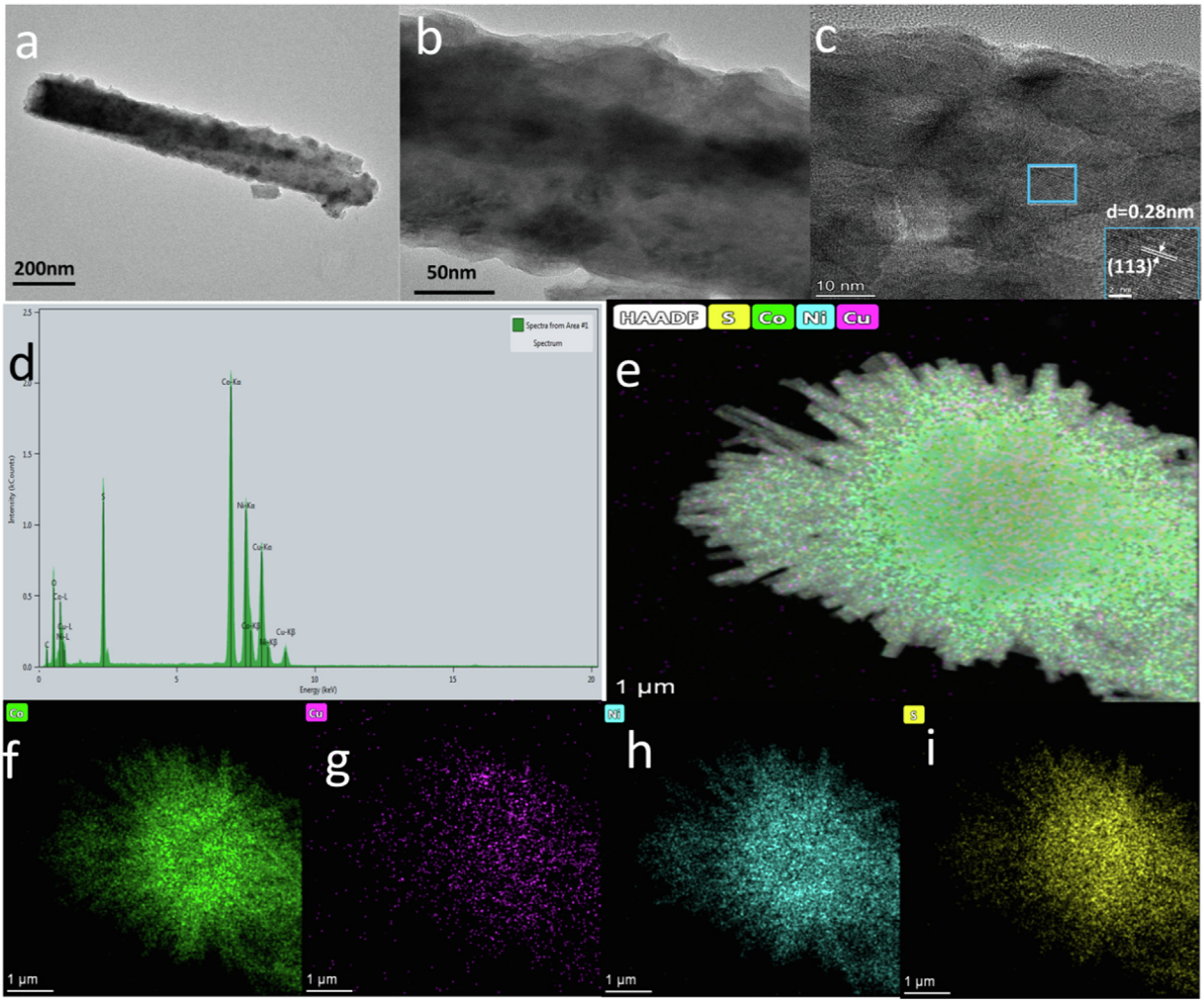

Fig. 4 (a–b) TEM image of PA@$CuCo_2S_4$/NF nanosheet. (c) The high-resolution TEM image of PA@$CuCo_2S_4$/NF nanowire. (d) TEM-EDX spectrum. (e–i) The HADDF image and EDX mapping of Cu, Co, Ni and S from PA@$CuCo_2S_4$/NF nanowire.

further confirms the successful preparation of PA@$CuCo_2S_4$/NF catalyst with a unique flower-like nanowire structure.

The surface elemental composition of the plasma-modified $CuCo_2S_4$/NF and its valence states were analyzed in depth using X-ray photoelectron spectroscopy (XPS). First, we used XPS full spectrum to confirm the presence of four elements in PA@$CuCo_2S_4$/NF (Fig. 5a), which is consistent with the above characterization results. The spectra of Cu 2p XPS with two spin orbitals Cu $2p_{3/2}$ and Cu $2p_{1/2}$ are shown in Fig. 5b. Deconvolution of these two orbitals generated four peaks at 932.5, 934.5, 952.4, and 954.7 eV. This indicated the presence of Cu in the sample as Cu^+ and Cu^{2+}, with areas filled with the same color in the figure. In addition, we detected the presence of two satellite peaks, which give the material outstanding charge-transfer rate (Zang et al., 2020). While fitting the Co 2p XPS spectra of PA@$CuCo_2S_4$/NF (Fig. 5c), we found that the peaks at 778.8 and 781.5 eV belonged to the Co $2p_{3/2}$ spin–orbital, as well as the peaks at 793.8 and 796.5 eV belonged to the Co $2p_{1/2}$ spin–orbital due to the presence of Co in the form of Co^{3+} and Co^{2+}. Moreover, the Co 2p XPS spectrum has identical number of satellite peaks as Cu 2p XPS. As shown in Fig. 5d, the peaks in the S 2p XPS spectra at 161.8 eV were assigned to the S $2p_{3/2}$ orbital, whereas the peaks at 162.9 eV were attributed to the S $2p_{1/2}$ orbital, which confirms the presence of S^{2-} in the composite. The S—O bond is responsible for the peak at 168.5 eV, and this is due to the inevitable reaction of S with the oxygen adsorbed onto the surface during the reaction, thereby forming some sulfate-like substances (Gautam et al., 2021; Zhao et al., 2021; Wang et al., 2022a, b). Thus, results from the XPS elemental and its chemical valence analysis indicate the successful preparation of DBD plasma-modified $CuCo_2S_4$/NF materials.

3.2. Hydrogen evolution reaction

In alkaline media, the HER properties of the produced materials were examined. Fig. 6a shows the polarization curves of all samples, which were tested using iR compensation to reduce the resistive overpotential. PA@$CuCo_2S_4$/NF exhibited the lowest onset potential and the fastest rate of curve drop. Furthermore, we investigated the material's HER activity by reading the overpotential corresponding to a current density of 10 mA cm^{-2}. As shown in Fig. 6b, compared with the measured overpotentials of $CuCo_2S_4$/NF, Co_3S_4/NF, Cu_2S/NF, and NF as comparison samples (149, 187, 249, and 280 mV, respectively), PA@$CuCo_2S_4$/NF had the lowest overpotential (107 mV). This indicates that the plasma modification further improves the catalytic activity of $CuCo_2S_4$/NF. We determined another crucial performance assessment criteria—Tafel slope—by fitting the polarization curve directly (Fig. 6c). PA@$CuCo_2S_4$/NF flower-like nanowires achieved the lowest Tafel slope (85.9 mV dec^{-1}) compared to other catalysts men-

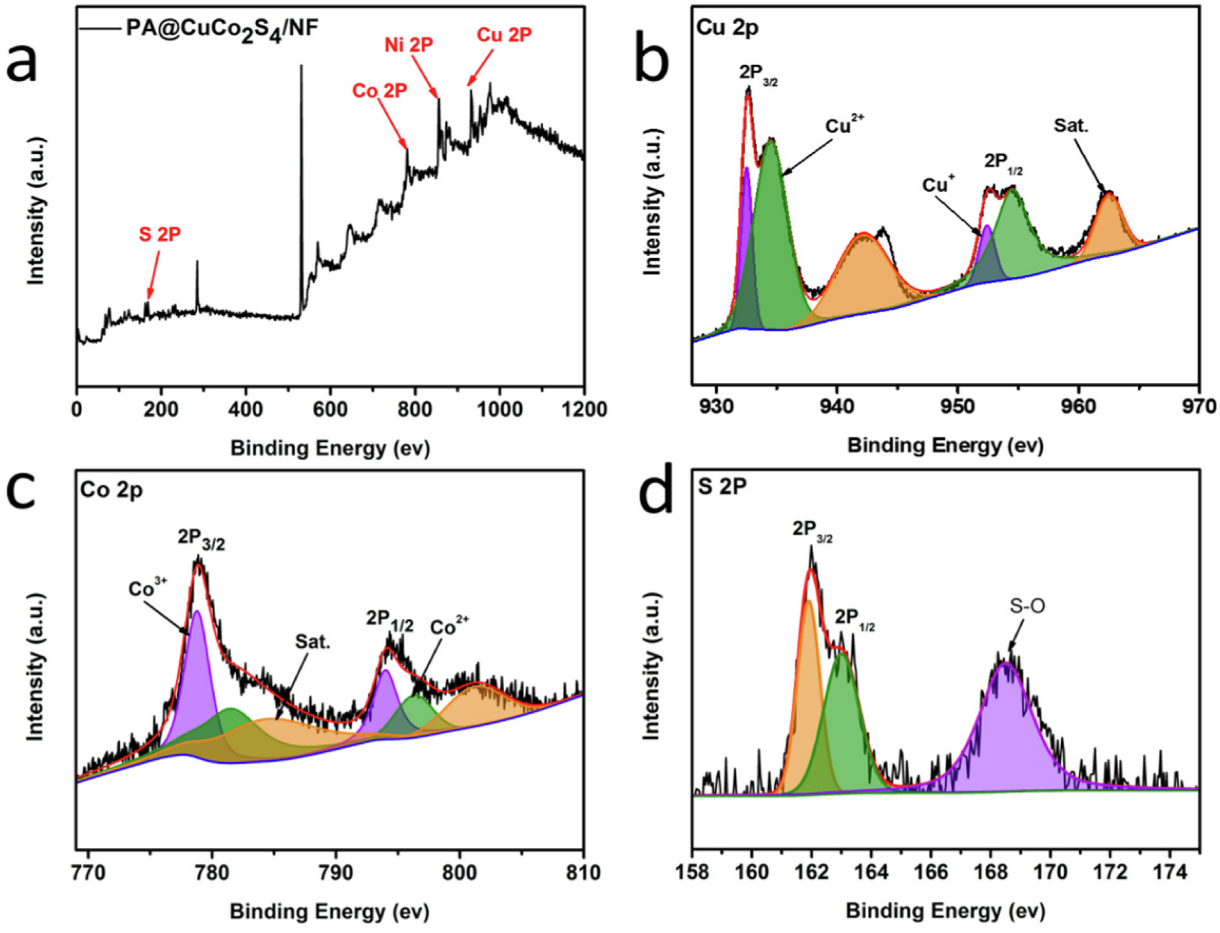

Fig. 5 (a) XPS survey spectra of PA@$CuCo_2S_4$/NF, XPS spectra of (b) Cu 2p, (c) Co 2p, (d) S 2p regions.

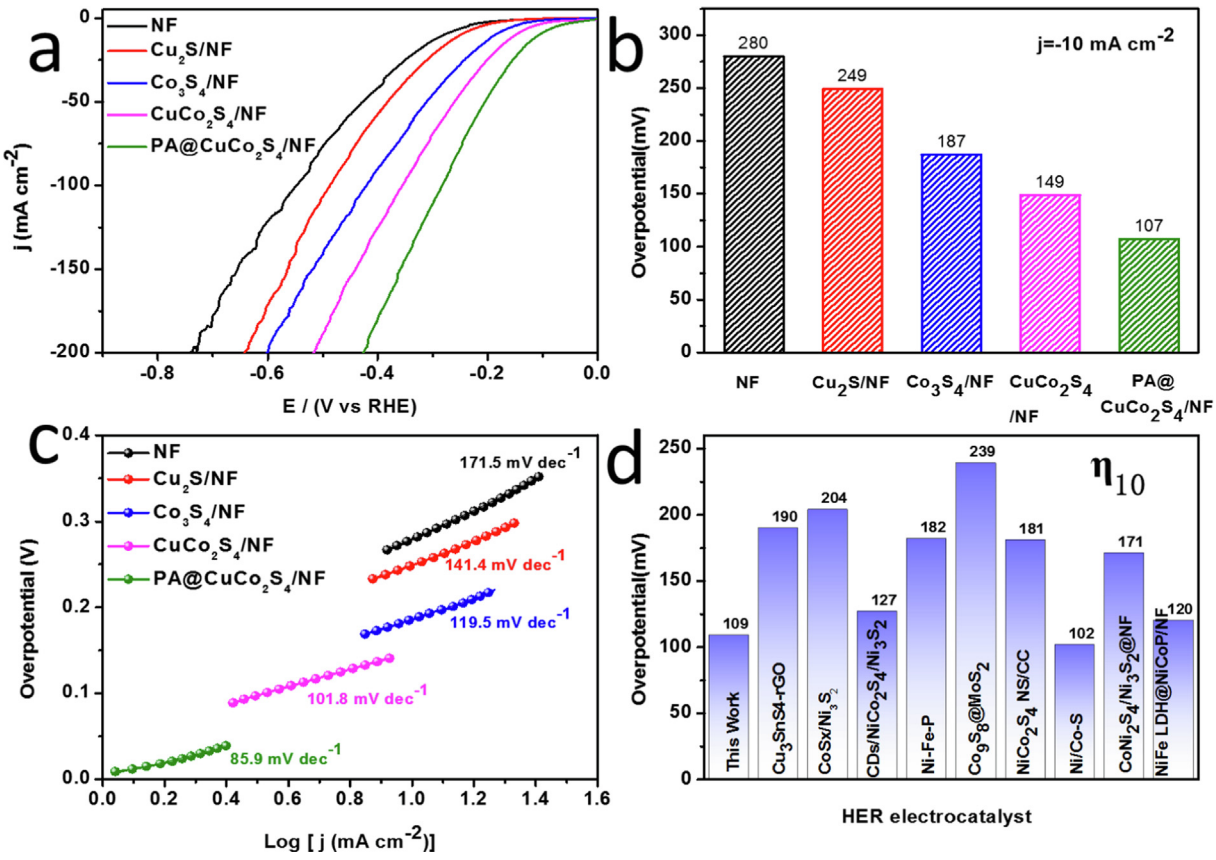

Fig. 6 HER performance of the prepared materials in 1.0 M KOH solution. (a) Polarization curves with 85% iR compensation. (b) Comparison of overpotentials for various catalysts at current densities of 10 mA cm^{-2} and (c) the Tafel plots. (d) Comparison of overpotential with other recently reported efficient electrocatalysts.

tioned before. Since PA@$CuCo_2S_4$/NF Tafel slope is between 40 and 120 mV dec^{-1}, we deduced that the hydrogen precipitation reaction occurs through the Volmer–Heyrovsky mechanism and Heyrovsky was the decisive step. Tafel results showed that PA@$CuCo_2S_4$/NF flower-like nanowires have optimal reaction kinetics and thus the fastest HER rate. In addition to comparing with the homemade samples, we also compared PA@$CuCo_2S_4$/NF with the reported transition metal sulfide phases using histograms (Fig. 6d). The overpotential value of PA@$CuCo_2S_4$/NF is smaller than most of the catalysts having similar current density. This indicates that PA@$CuCo_2S_4$/NF has the best HER activity and hence, increases the hydrogen production rate and reduces energy consumption.

The electrochemically-active surface area has a linear relationship with the electrochemical double-layer capacitance (C_{dl}), so the C_{dl} values are frequently compared directly. The linear cyclic voltammetric curves were recorded at different sweep speeds. The last turn of CV curve data at each rate was plotted for stable and reliable results. Normally, as the scan rate increases, the anode and cathode current densities of the CV curve as well as the Δj value increase. Curves of different sweep speeds and the corresponding Δj values were plotted in Fig. 7a. The slope of these curves represents the electrochemical double-layer capacitance value. The pure NF showed the lowest C_{dl} value (3.8 mF cm^{-2}). Furthermore, the C_{dl} value increased considerably after Cu and Co doping, indicating that nanowires have a larger surface area than the bulk structures. Bimetallic doping further increased the surface area of the catalyst, resulting in a C_{dl} value of $CuCo_2S_4$/NF that is about twice that of Co_3S_4/NF (128.7 mF cm^{-2}). Moreover, plasma bombardment helped to realize the maximum C_{dl} value (143.1 mF cm^{-2}) of PA@$CuCo_2S_4$/NF, which was 38 times that of NF. The electrochemical bilayer capacitance results show that the plasma-modified flower-like nanowire catalysts have the largest electrochemical active surface area, implying that they have more active sites.

We tested electrochemical impedance spectra at a fixed voltage to further probe the reaction kinetics on the material surface. The electrochemical impedance spectrum of each material is an approximately semicircular curve from which their R_{ct} can be calculated (Fig. 7b). Pure nickel foam has an R_{ct} of nearly 50 Ω; whereas PA@$CuCo_2S_4$/NF flowery nanowires have an R_{ct} of only 1.8 Ω. These results reveal that the PA@$CuCo_2S_4$/NF catalyst has a faster electron transport rate, which is one of the reasons for its splendid catalytic activity. The fast reaction kinetics were due to the following aspects: direct catalyst growth on NF was superior to dropping the material directly on NF because it allows the material to attach tightly to the substrate and accelerate charge transfer; plasma bombardment gave catalysts unique flower-like nanowire structures; and the crater formation due to the bombardment were observed at high magnification, which also played an effective role in charge transfer.

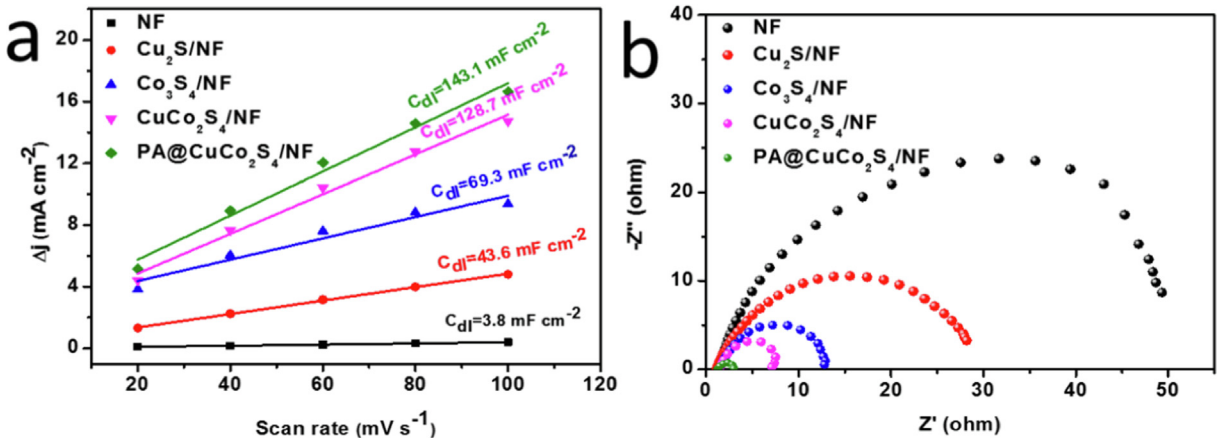

Fig. 7 (a) Estimation of C_{dl} by plotting the current density variation ($\Delta j = (ja - jc)/2$). (b)Nyquist plots of various catalysts.

The design of HER catalysts for practical production applications must focus on the electrocatalytic activity of the material and its stability. We primarily discuss the stability of PA@$CuCo_2S_4$/NF flower-like nanowires using two methods: one is the polarization curve before and after 1000 CV cycles, and the other is the chronocurrent method. The CV cycle was performed at a sweep rate of 100 mV s^{-1}, and the polarization curve was obtained at the end with 85% iR compensation., the black line represents the original curve, and the red line represents the curve after 1000 cycles, as shown in Fig. 8a. The curve expanded slightly and is almost negligible. A timing current test was also performed at a fixed voltage (Fig. 8b). After 20 h of testing, PA@$CuCo_2S_4$/NF current density increased only slightly. Both tests indicated the good stability of the catalysts, which was mainly attributed to the solid growth of the flower-like nanowires that were obtained via plasma modification on NF.

3.3. Oxygen evolution reaction

Compared with HER, the electron transfer process of OER was more complex and the kinetic process was slower, which greatly influenced the efficiency of the electrolytic water splitting. Therefore, we tested the OER performance of the material using the same three-electrode system. For comparison, we also performed OER performance tests on $CuCo_2S_4$/NF, Co_3S_4/NF, Cu_2S/NF, and NF samples. First, we conducted several linear cyclic voltammetry tests at a sweep rate of 100 mV s^{-1} to activate the material. Then, the polarization curves of the material were analyzed using linear scanning voltammetry (Fig. 9a) with 85% iR compensation as HER. Fig. 9a shows that all catalyst polarization curves have distinct raised peaks, which are mainly attributed to the oxidation peaks of nickel in NF substrates and is consistent with other literature (Feng et al., 2021; Liu et al., 2020; Hu et al., 2020). Compared with other materials, the PA@$CuCo_2S_4$/NF catalyst has low overpotential and a faster rise in the curve. Fig. 9b shows the OER overpotential of all catalysts; NF had the highest overpotential (407 mV), proving that the catalyst performance is mainly affected by the composite material on the NF. The overpotential of the $CuCo_2S_4$/NF (150 mV) was lower than that of Co_3S_4/NF and Cu_2S/NF and is due to the coordination effect between the bimetal. The plasma modification further increased the activity of the catalyst, with PA@$CuCo_2S_4$/NF having the lowest overpotential (110 mV) compared to the other samples. The Tafel slope is an important parameter to evaluate the OER kinetic process of a mate-

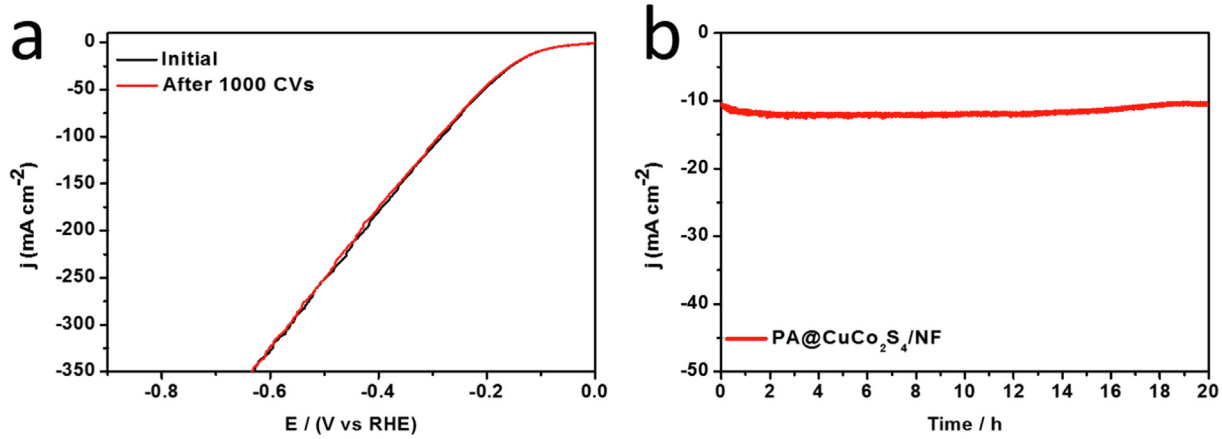

Fig. 8 (a) HER polarization curves of PA@$CuCo_2S_4$/NF before and after 1000 CV tests. (b) Chronoamperometric plot of PA@$CuCo_2S_4$/NF material for 20 h.

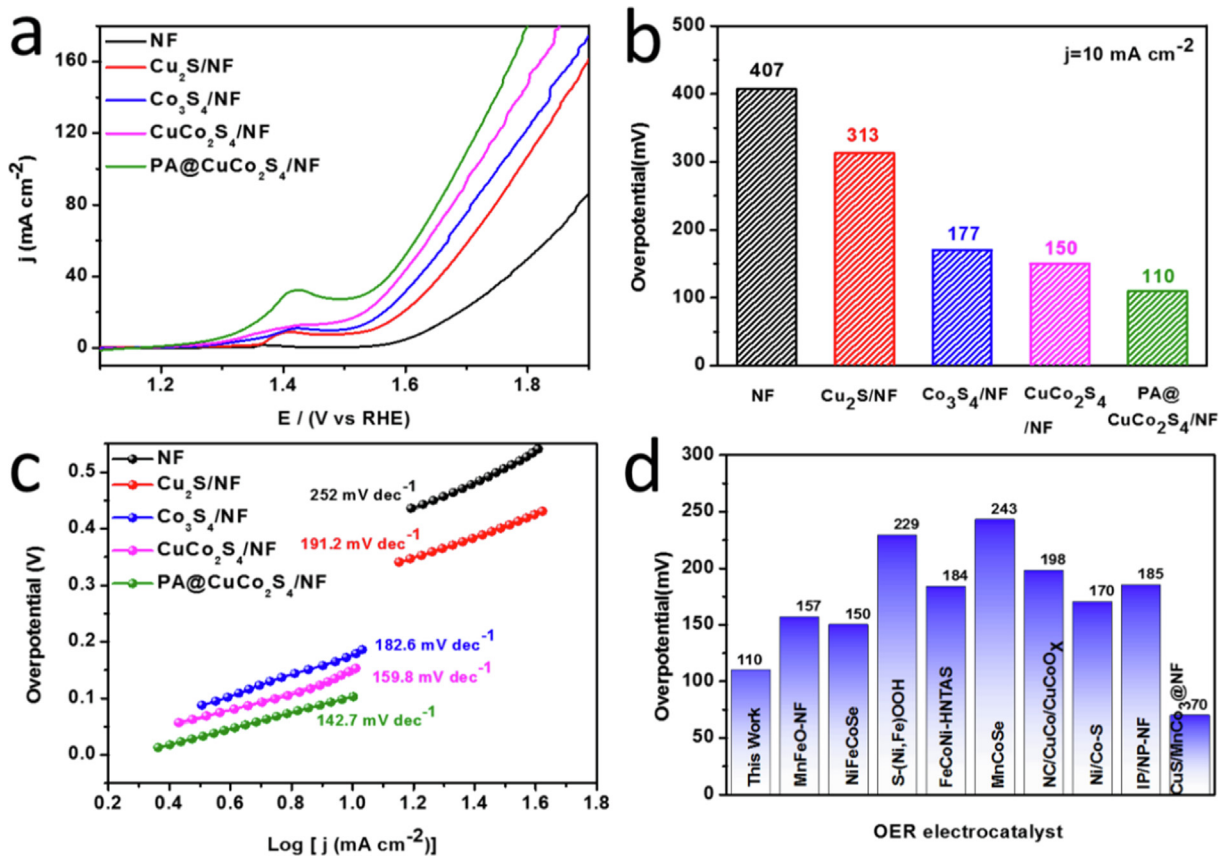

Fig. 9 OER performance of the prepared materials in 1.0 M KOH solution. (a) Polarization curves with 85% iR compensation. (b) Comparison of overpotentials for various catalysts at current densities of 10 mA cm^{-2} and (c) the Tafel plots. (d) Comparison of overpotential with other recently reported efficient electrocatalysts.

rial. Tafel plots fitted using polarization curves are presented in Fig. 9c. The Tafel slopes of $CuCo_2S_4$/NF, Co_3S_4/NF, Cu_2S/NF, and NF were 252 mV dec^{-1}, 191.2 mV dec^{-1}, 182.6 mV dec^{-1}, and 159.8 mV dec^{-1}, respectively; all of them were higher than that of PA@$CuCo_2S_4$/NF flower-like nanowires (142.7 mV dec^{-1}). The minimal Tafel slope allows PA@$CuCo_2S_4$/NF to have the fastest reaction kinetics, favoring the rapid diffusion of oxygen. Additionally, we demonstrated that plasma-modified $CuCo_2S_4$/NF catalysts outperformed most transition metal composites (Fig. 9d): MnFeO–NF (157 mV) (Luo et al., 2020), NiFeCoSe (150 mV) (Chi et al., 2017), S—(Ni,Fe)OOH (229 mV) (Yu et al., 2020), FeCoNi–HNTAs (184 mV) (Li et al., 2018), and IP/NP-NF (185 mV) (Xu et al., 2019), etc.

The activity of the material directly affects the magnitude of the ECSA, and can be evaluated by calculating the double-layer capacitance, which is linearly related to it. Fig. 10a shows the different scan rates fitted to the corresponding current densities; furthermore the slope of the fitted line is C_{dl}. All current densities are obtained from the CV plots in the nonFaraday interval. The double-layer capacitance of Ni foam, Cu_2S/NF, Co_3S_4/NF, and $CuCo_2S_4$/NF were 3.5, 37.2, 39.8, and 57.3 mF cm^{-2}, respectively. Among them, the PA@$CuCo_2S_4$/NF flower-like nanowires had the largest C_{dl} value (70.1 mF cm^{-2}). Therefore, it can be concluded that PA@$CuCo_2S_4$/NF has the largest specific surface area, leading to large number of active sites thus effectively increasing the OER catalytic activity.

The OER were further investigated using EIS). The Nyquist plot for all materials is presented in Fig. 10b. The NF demonstrated a maximum R_{ct} of 66.5 Ω, consistent with the HER results. We have also zoomed in on the EIS curves of Co_3S_4/NF, $CuCo_2S_4$/NF, and PA@$CuCo_2S_4$/NF in Fig. 10c for closer inspection. The R_{ct} of Cu_2S/NF (20.2 Ω), Co_3S_4/NF (6.0 Ω), and $CuCo_2S_4$/NF(4.1 Ω) were lower than that of NF, suggesting that Co plays a crucial role in $CuCo_2S_4$/NF catalyst. Furthermore, PA@$CuCo_2S_4$/NF exhibited the lowest R_{ct} value (2.5 Ω). The unique flower-like nanowire morphology of PA@$CuCo_2S_4$/NF facilitated the efficient charge transfer, resulting in the fastest Faraday process during OER.

In addition to the catalytic activity, the stability of the material is also an important factor to consider. PA@$CuCo_2S_4$/NF flower-like nanowires were tested in alkaline solutions to investigate their stability. Similar to the HER test method, the OER polarization curve was also tested before and after 1000 CV cycles, and the results were compared. As shown in Fig. 11a, there was almost no deviation between the two polarization curves, indicating that the PA@$CuCo_2S_4$/NF material has superb good cycling performance. Furthermore, the stability of the material was tested using Chronoamperometric plots at a constant overpotential of 120 mV (Fig. 11b). The current density of the PA@$CuCo_2S_4$/NF material remained constant

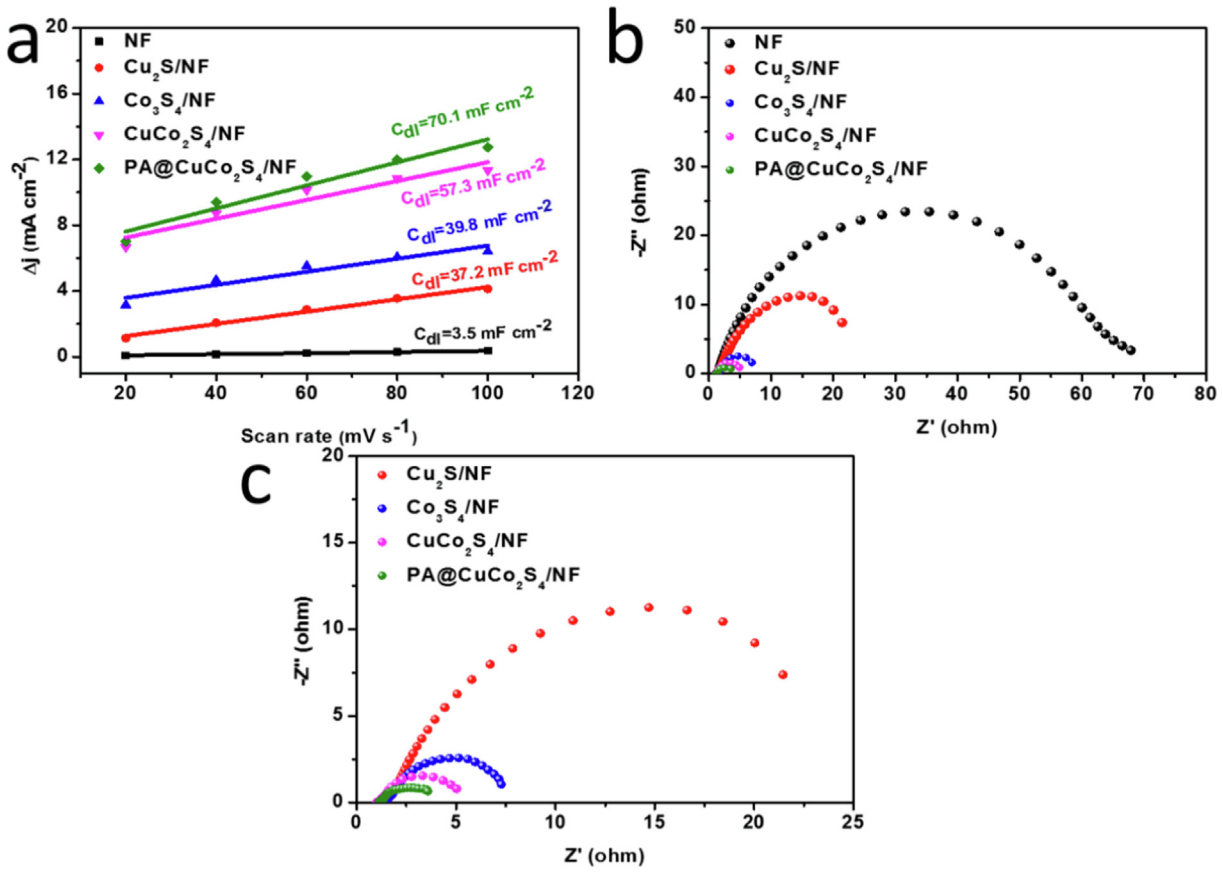

Fig. 10 (a) Estimation of C_{dl} by plotting the current density variation ($\Delta j = (ja - jc)/2$). (b–c) Nyquist plots of various catalysts.

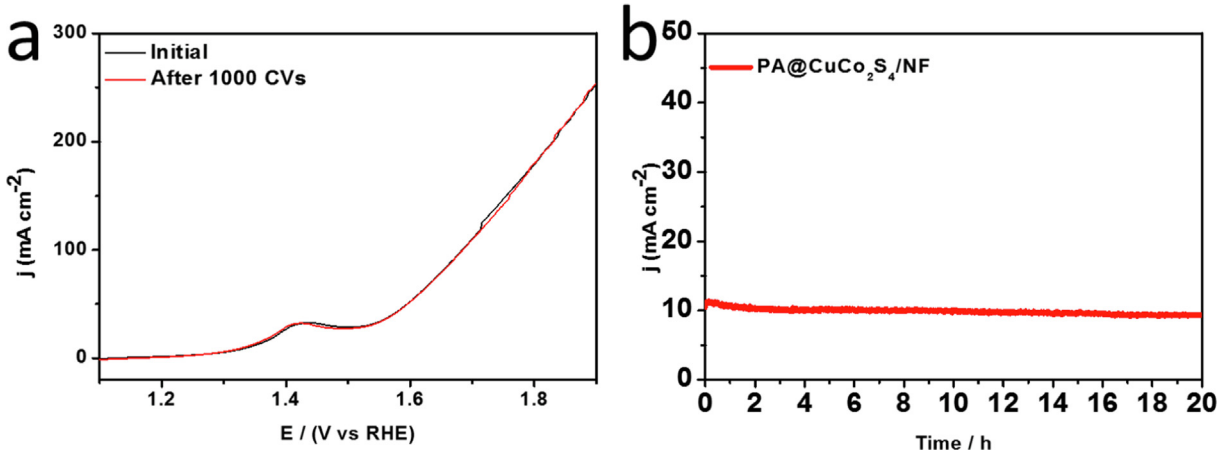

Fig. 11 (a) OER polarization curves of PA@$CuCo_2S_4$/NF before and after 1000 CV tests. (b) Chronoamperometric plot of PA@$CuCo_2S_4$/NF material for 20 h.

for 20 h, demonstrating its long-lasting catalytic activity during the oxygen precipitation reaction.

3.4. Overall water splitting

The study demonstrated that PA@$CuCo_2S_4$/NF flower-like nanowires exhibited remarkable catalytic activity and stability for HER and OER; therefore, we used them as cathodes and anodes for the overall water splitting reactions to investigate their catalytic activities. Similarly, $CuCo_2S_4$/NF, Co_3S_4/NF, Cu_2S/NF, and NF were tested as comparisons. Fig. 12a shows a simple device for the overall water splitting. The researchers used a 1 M KOH alkaline electrolyte, and the catalyst with an area of 1 cm^2 is held by two working electrode clamps. H_2, and O_2 were generated on the both electrodes after applying an external voltage. The polarization curves for the overall water splitting reaction were tested using an electrochemical work-

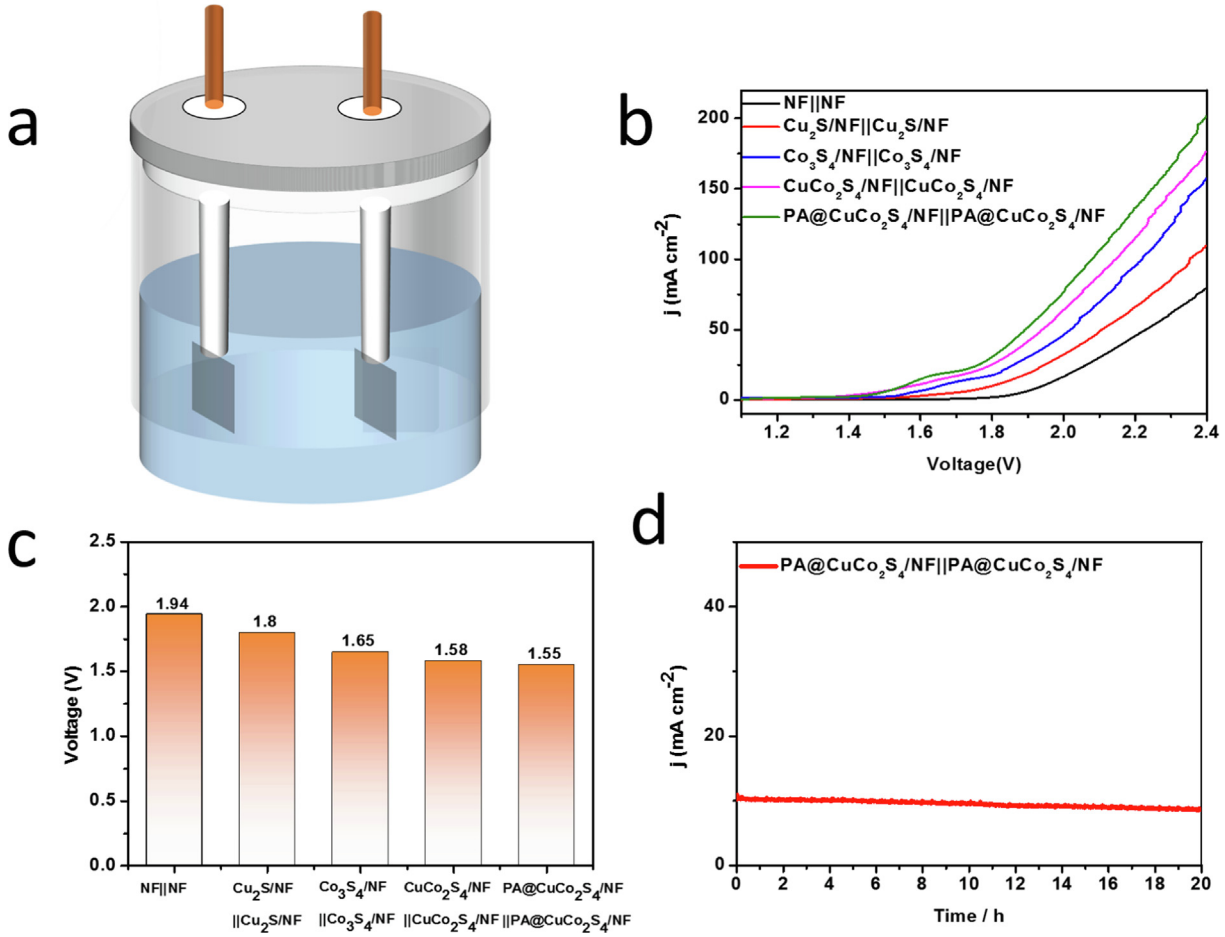

Fig. 12 (a) PA @ $CuCo_2S_4$/NF (a) | | PA @ $CuCo_2S_4$/NF double electrode structure diagram of the overall water splitting, (b) polarization curves of all catalysts for overall water splitting in 1 M KOH with a scan rate of 5 mV S^{-1}, (c) The voltage required for all catalysts to drive the 10 mA cm^{-2} current density, (d) Chronoamperometric plot recorded at PA@$CuCo_2S_4$/NF||PA@$CuCo_2S_4$/NFunder 1.6 V voltage.

station, and the highest current density was consistently obtained for PA@$CuCo_2S_4$/NF||PA@$CuCo_2S_4$/NF at the same voltage compared to other materials (Fig. 12b). Undoubtedly, PA@$CuCo_2S_4$/NF|| PA@$CuCo_2S_4$/NF has the lowest battery voltage of only 1.55 V, whereas $CuCo_2S_4$/NF|| $CuCo_2S_4$/NF, Co_3S_4/NF||Co_3S_4/NF, Cu_2S/NF||Cu_2S/NF, NF||NF requires 1.58, 1.65, 1.8, and 1.94 V, respectively (Fig. 12c). Furthermore, the battery voltage of PA@$CuCo_2S_4$/NF||PA@$CuCo_2S_4$/NF was slightly better than the other reported nickel foam-based bifunctional catalysts, as shown in Table 1.

We also measured the time–current curves of PA@$CuCo_2S_4$/NF|| PA@$CuCo_2S_4$/NF to investigate the stability of the two-electrode system (Fig. 12d). At constant voltage (1.6 V),

Table 1 The comparison of OWS performance between IP/NP-NF and other recently reported bifunctional catalysts on NF in 1 M KOH.

Materials	Cell voltage (V)	Ref.
PA@$CuCo_2S_4$/NF	1.55 V	This Work
Fe-Co-Ni-Sx/NF	1.7 V	Zhu et al., 2022a,b
Fe-Co-P-Gr/NF	1.58 V	Wang et al., 2020
NiCoP/NF	1.6 V	Wang et al., 2021
CoO/NF	1.76 V	Zhu et al., 2020a,b
Co_9S_8/2H-WS_2@NF	1.58 V	Wang et al., 2022a,b
POM@ZnCoS/NF	1.56 V	Gautam et al., 2021
NiFeOH/CoSx/NF	1.563 V	Bose et al., 2020
NiFe-200@Co(OH) NSAs/NF	1.58 V	Cheng et al., 2021
NiFeMo/NF	1.62 V	Wang et al., 2023a,b

the material maintained reliable stability with only a slight drop in current density around 10 mA cm^{-2} for 20 h. Therefore, we prepared a bifunctional catalyst with high catalytic activity and durability, and promising future in practical production applications. The excellent performance of the catalyst benefits from four main aspects: the use of 3D structured NF as a substrate successfully reduces the resistance between the material and the medium, increases electrical conductivity, and accelerates mass/electron transfer and the release of reaction products; the bimetal synergize with each other in the reaction, effectively improving the intrinsic activity; the DBD plasma modification further increases the electrochemical specific surface area of the material, exposing more active sites and accelerating the reaction kinetics; and the unique flower-like nanowire structure firmly grown on the 3D NF gives it better durability during the reactions.

4. Conclusions

In summary, we successfully synthesized uniformly-distributed $CuCo_2S_4$/NF nanowire arrays and then modified them using plasma technology to obtain outstanding bifunctional catalysts with unique flower-like nanowire structures. We tested the HER and OER catalytic activities of PA@$CuCo_2S_4$/NF in an alkaline medium. Results show that the catalyst requires overpotential of only 107 mV to realize a current density of 10 mA cm^{-2} in HER; furthermore, the fitted Tafel curves show that PA@$CuCo_2S_4$/NF has the lowest Tafel slope. PA@$CuCo_2S_4$/NF only requires overpotential of 110 mV in the OER to supply an anode current of 10 mA cm^{-2}. Also, we investigate its activity as a bifunctional catalyst in an alkaline electrolyzer. PA@$CuCo_2S_4$/NF demonstrated that it only requires an applied voltage of 1.55 V during the overall water splitting. We found that the catalyst possess good stability during HER, OER, and overall water splitting in the 20-hour chronocurrent test. Therefore, we not only propose a low-cost and superior bifunctional catalyst, but also present a novel method for catalyst preparation in electrolytic water in this study. Moreover, this result further promotes the application of DBD plasma modification technology for water splitting.

Declaration of Competing Interest

The authors declare that they have no known competing financial interests or personal relationships that could have appeared to influence the work reported in this paper.

Acknowledgments

This work was supported by the National Natural Science Foundation of China (No. 21246010), the Key Natural Science Foundation of the Jiangsu Higher Education Institutions of China (Grant No. 22KJA610001) and supported by Science and Technology Project Fund of Nantong (JC2021163) and Changzhou Institute of Technology High level Talent Launch Project (YN22010).

References

Bose, R., Jothi, V.R., Karuppasamy, K., Alfantazi, A., Yi, S.C., 2020. High performance multicomponent bifunctional catalysts for overall water splitting. J. Mater. Chem. A 8, 13795–13805.

Cen, J.M., Shen, P.K., Zeng, Y.F., 2021. Ru doping NiCoP heteronanowires with modulated electronic structure for efficient overall water splitting. J. Colloid Interface Sci. 610, 213–220.

Chen, X., Yu, M., Yan, Z.H., Guo, W., Fan, G.L., Ni, Y.X., Liu, J.D., Zhang, W., Xie, W., Cheng, F.Y., Chen, J., 2020. Boosting electrocatalytic oxygen evolution by cation defect modulation via electrochemical etching. CCS Chem. 2, 675–685.

Cheng, C., Liu, F.Y., Zhong, D.Z., Hao, G.Y., Liu, G., Li, J.P., Zhao, Q., 2021. Three-dimensional self-supporting catalyst with NiFe alloy/oxyhydroxide supported on high-surface cobalt hydroxide nanosheet array for overall water splitting. J. Colloid Interface Sci. 606, 873–883.

Chi, J.Q., Yan, K.L., Xiao, Z., Dong, B., Shang, X., Gao, W.K., Li, X., Chai, Y.M., Liu, C.G., 2017. Trimetallic Ni-Fe-Co selenides nanoparticles supported on carbon fifiber cloth as effifficient electrocatalyst for oxygen evolution reaction. Int. J. Hydrogen Energy 42 (32), 20599–20607.

Czioska, S., Wang, J.Y., Teng, X., 2018. Hierarchically structured $CuCo_2S_4$ nanowire arrays as efficient bifunctional electrocatalyst for overall water splitting. ACS Sustain. Chem. Eng. 6 (9), 11877–11883.

Duan, D.H., Guo, D.S., Gao, J., Liu, S.B., Wang, Y.F., 2022. Electrodeposition of cobalt-iron bimetal phosphide on Ni foam as a bifunctional electrocatalyst for efficient overall water splitting. J. Colloid Interface Sci. 622, 250–260.

Feng, X.J., Shi, Y.L., Shi, J.H., Hao, L.H., Hu, Z.G., 2021. Superhydrophilic 3D peony flower-like Mo-doped Ni_2S_3@NiFe LDH heterostructure electrocatalyst for accelerating water splitting. Int. J. Hydrogen Energy 46 (7), 5169–5180.

Gautam, J., Liu, Y., Gu, J., Ma, Z.Y., Zha, J.J., Dahal, B., Zhang, L. N., Chishti, A.N., Ni, L., Diao, G.W., Wei, Y.G., 2021. Fabrication of polyoxometalate anchored zinc cobalt sulfide nanowires as a remarkable bifunctional electrocatalyst for overall water splitting. Adv. Funct. Mater. 31 (46), 2106147.

Guo, Y., Park, T., Yi, J.W., Henzie, J., Kim, J.H., Wang, Z.L., Jiang, B., Bando, Y., Yamauchi, Y., 2019. Nanoarchitectonics for transition-metal-sulfide-based electrocatalysts for water splitting. Adv. Mater. 31, (17) 1807134.

Han, N., Liu, P.Y., Jiang, J., Ai, L.H., Shao, Z.P., Liu, S.M., 2018. Recent advances in nanostructured metal nitrides for water splitting. J. Mater. Chem. A 6, 19912–19933.

Hu, J., Zhu, S.L., Liang, Y.Q., Li, Z.Y., Luo, S.Y., Cui, Z.D., 2020. Self-supported Ni_3Se_2@NiFe layered double hydroxide bifunctional electrocatalyst for overall water splitting. J. Colloid Interface Sci. 587, 79–89.

Li, H.Y., Chen, S.M., Zhang, Y., Zhang, Q.H., Jia, X.F., Zhang, Q., Gu, L., Sun, X.M., Song, L., Wang, X., 2018. Systematic design of superaerophobic nanotubearray electrode comprised of transition-metal sulfifides for overall water splitting. Nat. Commun. 9, 2452.

Li, D.Y., Liao, L.L., Zhou, H.Q., Zhao, Y., Cai, F.M., Zeng, J.S., Liu, F., Wu, H., Tang, D.S., Yu, F., 2021b. Highly active non-noble electrocatalyst from Co_2P/Ni_2P nanohybrids for pH-universal hydrogen evolution reaction. Mater. Today Phys. 16, 100314.

Li, C.F., Zhao, J.W., Xie, L.J., Wu, J.Q., Li, G.R., 2021a. Fe doping and oxygen vacancy modulated Fe-Ni_5P_4/NiFeOH nanosheets as bifunctional electrocatalysts for efficient overall water splitting. Appl. Catal. B Environ. 291, 119987.

Liu, J.L., Gao, Y., Tang, X.X., Zhan, K., Zhao, B., Xia, B.Y., Yan, Y., 2020. Metal-organic framework-derived hierarchical ultrathin CoP nanosheets for overall water splitting. J. Mater. Chem. A 8, 19254–19261.

Liu, J., Yuan, H., Wang, Z., Li, J., Yang, M.Y., Cao, L.J., Liu, G.Y., Qian, D., Lu, Z.J., 2019. Self supported nickel iron oxide nanospindles with high hydrophilicity for efficient oxygen evolution. Chem. Commun. 55 (73), 10860–10863.

Luo, J., Guo, W.H., Zhang, Q., Wang, X.H., Shen, L., Fu, H.C., Wu, L.L., Chen, X.H., Luo, H.Q., Li, N.B., 2020. One-pot synthesis of Mn-Fe bimetallic oxide heterostructures as bifunctional electrodes for effifficient overall water splitting. Nanoscale 12, 19992–20001.

Ma, H.B., Chen, Z.W., Wang, Z.L., Singh, C.V., Jiang, Q., 2022. Interface engineering of co/comon/nf heterostructures for high-

performance electrochemical overall water splitting. Adv. Sci. 9, (11) 2105313.
Shang, L., Zhao, Y.X., Kong, X.Y., Shi, R., Waterhouse, G.I.N., Wen, L.P., Zhang, T.R., 2020. Underwater superaerophobic Ni nanoparticle- decorated nickel molybdenum nitride nanowire arrays for hydrogen evolution in neutral media. Nano Energy 78, 105375–105381.
Song, M., Zhang, Z.J., Li, Q.W., Jin, W., Wu, Z.X., Fu, G.T., Liu, X. E., 2019. Ni-foam supported Co(OH)F and Co-P nanoarrays for energy-efficient hydrogen production via urea electrolysis. J. Mater. Chem. A 7, 3697–3703.
Wang, Z.L., Chen, H.X., Bao, J., Song, Y.H., She, X.J., Lv, G.A., Deng, J.J., Li, H.M., Xu, H., 2023b. Amorphized core-shell NiFeMo electrode for efficient bifunctional water splitting. Appl. Surf. Sci. 607, 154803.
Wang, J.J., Song, Y.C., Zuo, C.J., Li, R., Zhou, Y.M., Zhang, Y.W., Wu, B., Huang, Y.Z., 2022a. An argyrophylla-like nanorods Co_9S_8/2H-WS_2@NF heterojunction with electrons redistribution as a highly efficient bifunctional electrocatalyst for overall water splitting. ChemCatChem 14, (3) e202101553.
Wang, K.H., Sun, K.L., Li, Z.H., Lv, Z.H., Yu, T.P., Liu, X., Wang, G.X., Xie, G.G., Jiang, L.H., 2020. Preparation of Fe-Co-P-Gr/NF coating via electroless composite plating as efficient electrocatalysts for overall water splitting. Electron. Mater. Lett. 16, 164–173.
Wang, Q., Xu, H., Qian, X.Y., He, G.Y., Chen, H.Q., 2022b. Sulfur vacancies engineered self-supported Co_3S_4 nanoflowers as an efficient bifunctional catalyst for electrochemical water splitting. Appl. Catal. B Environ. 322, 122104.
Wang, D.D., Zhang, Y.W., Fei, T., Mao, C.F., Song, Y.C., Zhou, Y. M., Dong, G.M., 2021. NiCoP/NF 1D/2D Biomimetic Architecture for Markedly Enhanced Overall Water Splitting. ChemElectroChem 8, 3064–3072.
Wang, Z.H., Zhou, T., Chen, Z., Gu, R.Z., Tao, J.W., Fan, Z.W., Guo, L.Y., Liu, Y.S., 2023a. Three-Dimensional Strawlike $MoSe_2$-Ni(Fe)Se electrocatalysts for overall water splitting. Inorg. Chem. 62 (6), 2894–2904.
Wu, Z.X., Nie, D.Z., Song, M., Jiao, T.T., Fu, G.T., Liu, X.E., 2019. Facile synthesis of Co-Fe-B-P nanochains as an efficient bifunctional electrocatalyst for overall water-splitting. Nanoscale 11, 7506–7512.
Xiao, Y.P., Chen, X., Li, T.L., Mao, Y.Y., Liu, C.L., Chen, Y.C., Wang, W.J., 2022. Mo-doped cobalt hydroxide nanosheets coupled with cobalt phosphide nanoarrays as bifunctional catalyst for efficient and high-stability overall water splitting. Int. J. Hydrogen Energy 47 (17), 9915–9924.
Xu, X., Tian, X.M., Zhong, Z., Kang, L.T., Yao, J.N., 2019. In-situ growth of iron/nickel phosphides hybrid on nickel foam as bifunctional electrocatalyst for overall water splitting. Appl. Surf. Sci. 424, 42–51.
Yan, K.L., Shang, X., Li, Z., Dong, B., Chi, J.Q., Liu, Y.R., Gao, W. K., Chai, Y.M., Liu, C.G., 2017. Facile synthesis of binary NiCoS nanorods supported on nickel foam as effificient electrocatalysts for oxygen evolution reaction. Int. J. Hydrogen Energy 42 (27), 17129–17135.
Yan, K.L., Qin, J.F., Lin, J.H., Dong, B., Chi, J.Q., Liu, Z.Z., Dai, F. N., Chai, Y.M., Liu, C.G., 2018. Probing the active sites of Co_3O_4 for acidic oxygen evolution reaction by mod-ulating Co^{2+}/Co^{3+} ratio. J. Mater. Chem. A 6, 5678–5686.
Yang, L.J., Li, H., Yu, Y., Wu, Y., Zhang, L., 2020a. Assembled 3D MOF on 2D nanosheets for self-boosting catalytic synthesis of N-doped carbon nanotube encapsulated metallic Co electrocatalysts for overall water splitting. Appl. Catal. B Environ. 271, 118939.
Yang, Z., Lin, Y., Jiao, F.X., Li, J.H., Wang, J.L., Gong, Y.Q., 2020b. In situ growth of 3D walnut-like nano-architecture Mo-Ni_2-P@NiFe LDH/NF arrays for synergistically enhanced overall water splitting. J. Energy Chem. 49, 189–197.
Yao, Y.L., He, J.M., Yang, X., Peng, L., Zhu, X.D., Li, K.S., Qu, M. N., 2022. Superhydrophilic/underwater superaerophobic self-supporting CuS/Cu foam electrode for efficient oxygen evolution reaction. Colloids Surf. A Physicochem. Eng. Aspects 634, 127934.
Yi, X.R., He, X.B., Yin, F.X., Chen, B.H., Li, G.R., Yin, H.Q., 2020. One-step synthesis of oxygen incorporated V-MoS_2 supported on partially sulfurized nickel foam as a highly active catalyst for hydrogen evolution. Int. J. Hydrogen Energy 45 (4), 2774–2784.
Yu, L., Wu, L.B., McElhenny, B., Song, S.W., Luo, D., Zhang, F.H., Yu, Y., Chen, S., Ren, Z.F., 2020. Ultrafast room-temperature synthesis of porous S-doped Ni/Fe (oxy)hydroxide electrodes for oxygen evolution catalysis in seawater splitting. Energy Environ. Sci. 13 (10), 3439–3446.
Zang, N., Wu, Z.X., Wang, J., Chen, Z.F., 2020. Rational design of Cu-Co thiospinel ternary sheet arrays for high efficient electrocatalytic water splitting. J. Mater. Chem. A 8, 1799–1807.
Zhang, Y., Guo, H.R., Li, X.P., Du, J., Ren, W.L., Song, R., 2021a. A 3D multi-interface structure of coral-like Fe-Mo-S/Ni_3S_2@NF using for high-efficiency and stable overall water splitting. Chem. Eng. J. 404, 126483.
Zhang, D.W., Jiang, L.J., Liu, Y.Y., Qiu, L.J., Zhang, J.M., Yuan, D. S., 2019. Ni_3S_2-MoSx nanorods grown on Ni foam as high efficient electrocatalysts for overall water splitting. Int. J. Hydrogen Energy 44, 17900–17908.
Zhang, Y.J., Liu, L., Wang, J.W., Yao, R., Wu, Y., Wang, M.H., Zhao, Q., Li, J.P., Liu, G., 2021b. Rational introduction of S and P in multi-stage electrocatalyst to drive a large-current-density water oxidation reaction and overall water splitting. J. Power Sources 518, 230757.
Zhang, Z., Pang, C.X., Xu, W.C., Liang, Y.Q., Jiang, H., Li, Z.Y., Wu, S.L., Zhu, S.L., Wang, H., Cui, Z.D., 2023. Synthesis and water splitting performance of FeCoNbS bifunctional electrocatalyst. J. Colloid Interface Sci. 638, 893–900.
Zhang, Q., Zhang, C.C., Liang, J.B., Yin, P.G., Tian, Y., 2017. Orthorhombic α-NiOOH nanosheet arrays: Phase conversion and efficient bifunctional electrocatalysts for full water splitting. ACS Sustainable Chem. Eng. 5 (5), 3808–3818.
Zhang, R.R., Zhang, Y.C., Pan, L., Shen, G.Q., Mahmood, N., Ma, Y.H., Shi, Y., Jia, W.Y., Wang, L., Zhang, X.W., Xu, W., Zou, J. J., 2018. Engineering cobalt defects in cobalt oxide for highly efficient electrocatalytic oxygen evolution. ACS Catal. 8 (5), 3803–3811.
Zhang, R.Z., Zhu, Z.Q., Lin, J.H., Zhang, K.F., Li, N., Zhao, C.J., 2020. Hydrolysis assisted in-situ growth of 3D hierarchical FeS/NiS/nickel foam electrode for overall water splitting. Electrochim. Acta 332, 135534.
Zhao, L.X., Ge, H.Y., Zhang, G.H., Wang, F.B., Li, G.D., 2021. Hierarchical Ni_3S_2-CoMoSx on the nickel foam as an advanced electrocatalyst for overall water splitting. Electrochim. Acta 387, 138538.
Zhu, S.S., Lei, J.L., Zhang, L.N., He, J.X., 2020a. CoO/NF nanowires promote hydrogen and oxygen production for overall water splitting in alkaline media. Int. J. Hydrogen Energy 45, 8031–8040.
Zhu, S.S., Lei, J.L., Zhang, L.N., He, J.X., 2020b. CoO/NF nanowires promote hydrogen and oxygen production for overall water splitting in alkaline media. Int. J. Hydrogen Energy 45 (12), 8031–8040.
Zhu, S.S., Lei, L.J., Wu, S.M., Liu, L., Chen, T.M., Yuan, Y., Ding, C., 2022a. Construction of Fe-Co-Ni-Sx/NF nanomaterial as bifunctional electrocatalysts for water splitting. Mater. Lett. 311, 131549.
Zhu, L.L., Li, C.D., Li, H., Li, H., Wu, Z.Q., Huang, Y.N., Zhu, X.B., Sun, Y.P., 2022b. Adjustable antiperovskite cobalt-based nitrides as efficient electrocatalysts for overall water splitting. J. Mater. Chem. A 10, 15520–15527.